arXiv:1203.4089v2 [physics.acc-ph] 23 Mar 2012

Preprint typeset in JINST style - HYPER VERSION

The MICE Muon Beam on ISIS and the beam-line instrumentation of the Muon Ionization Cooling Experiment

---

The MICE Collaboration

M. Bogomilov, Y. Karadzhov [1], D. Kolev, I. Russinov, R. Tsenov, G.Vankova-Kirilova

Department of Atomic Physics, St. Kliment Ohridski University of Sofia, Sofia, Bulgaria
[1] *Now at DPNC, Université de Genève, Geneva, Switzerland*

L. Wang, F.Y. Xu, S.X. Zheng

Institute for Cryogenic and Superconductivity Technology, Harbin Institute of Technology, Harbin, PR China

R. Bertoni, M. Bonesini ,[*] F. Ferri [2], G. Lucchini, R. Mazza, F. Paleari [3], F. Strati

Sezione INFN Milano Bicocca, Dipartimento di Fisica G. Occhialini, Milano, Italy
[2] *Present address DSM/IRFU, CEA/Saclay, Gif-sur-Yvette, France*
[3] *Now at Quanta Systems, Solbiate Olona, Varese, Italy*

V. Palladino

Sezione INFN Napoli and Dipartimento di Fisica, Università Federico II, Complesso Universitario di Monte S. Angelo, Napoli, Italy

G. Cecchet, A. de Bari

Sezione INFN Pavia and Dipartimento di Fisica Nucleare e Teorica, Pavia, Italy

M. Capponi, A. Cirillo, A. Iaciofano, A. Manfredini, M. Parisi, D. Orestano, F. Pastore, A. Tonazzo [4], L. Tortora

Sezione INFN Roma Tre e Dipartimento di Fisica, Roma, Italy
[4] *Present address APC, Universitè Paris Diderot, Paris, France*

Y. Mori

Kyoto University Research Reactor Institute, Osaka, Japan

Y. Kuno, H. Sakamoto, A. Sato, T. Yano, M. Yoshida

Osaka University, Graduate School of Science, Department of Physics, Toyonaka, Osaka, Japan

S. Ishimoto, S. Suzuki, K. Yoshimura

High Energy Accelerator Research Organization (KEK), Institute of Particle and Nuclear Studies, Tsukuba, Ibaraki, Japan

F. Filthaut [5]

NIKHEF, Amsterdam, The Netherlands
[5] *Also at Radboud University Nijmegen, Nijmegen, The Netherlands*

R. Garoby, S. Gilardoni, P. Gruber, K. Hanke, H. Haseroth, P. Janot, A. Lombardi, S. Ramberger, M. Vretenar

CERN, Geneva, Switzerland

P. Bene, A. Blondel, F. Cadoux, J.-S. Graulich, V. Grichine[6]**, E. Gschwendtner**[7]**, F. Masciocchi, R. Sandstrom, V. Verguilov, H. Wisting**

DPNC, Section de Physique, Université de Genève, Geneva, Switzerland
[6] *Also at Lebedev Physical Institute, Moscow, Russia*
[7] *Now at CERN, Geneva, Switzerland*

C. Petitjean

Paul Scherrer Institut, Villigen, Switzerland

R. Seviour

The Cockcroft Institute, Daresbury Science and Innovation Centre, Daresbury, Cheshire, UK

J. Alexander, G. Charnley, N. Collomb, S. Griffiths, B. Martlew, A. Moss, I. Mullacrane, A. Oates, P. Owens, C. White, S. York

STFC Daresbury Laboratory, Daresbury, Cheshire, UK

D. Adams, R. Apsimon, P. Barclay, D.E. Baynham, T.W. Bradshaw, M. Courthold, P. Drumm [8]**, R. Edgecock, T. Hayler, M. Hills**[9]**, Y. Ivaniouchenkov, A. Jones, A. Lintern, C.MacWaters, C. Nelson, A. Nichols, R. Preece, S. Ricciardi, J.H. Rochford** [10]**, C. Rogers, W. Spensley** [11]**, J. Tarrant, K. Tilley, S. Watson, A. Wilson**

STFC Rutherford Appleton Laboratory, Harwell Oxford, Didcot, UK
[8] *Now at Space Research Centre, Department of Physics and Astronomy, University of Leicester, Leicester, UK*
[9] *Now at Mullard Space Science Laboratory, University College London, Dorking, Surrey, UK*
[10] *Now at Global Research Centre, General Electric, Albany, NY, USA*
[11] *Now at MANTEC SYSTEM Ltd., Newcastle Upon Tyne, UK*

D. Forrest, F.J.P. Soler, K. Walaron [12]

School of Physics and Astronomy, Kelvin Building, The University of Glasgow, Glasgow, UK
[12] *Also at Imperial College London, London, UK*

P. Cooke, R. Gamet

Department of Physics, University of Liverpool, Liverpool, UK

A. Alecou, M. Apollonio [13], G. Barber, R. Benselinck, D. Clark, I. Clark, D. Colling, A. Dobbs, P. Dornan, S. Fayer, A. Fish [14], R. Hare, S. Greenwood, A. Jamdagni, V. Kasey, M. Khaleeq, J. Leaver, K. Long, E. McKigney [15], T. Matsushita [16], J. Pasternak, T. Sashalmi, T. Savidge, M. Takahashi [17]

Department of Physics, Blackett Laboratory, Imperial College London, London, UK

[13] *Now at Diamond Light Source, Harwell Science and Innovation Campus, Didcot, Oxfordshire, UK*
[14] *BC asset management Ltd., BC House, Poole, Dorset, UK*
[15] *Now at Los Alamos Natl. Lab., Los Alamos, USA*
[16] *Now at Kobe University, Faculty of Science, 1-1 Rokkodai-cho, Nada-ku, Kobe-shi, Japan*
[17] *Now at School of Physics and Astronomy, University of Manchester, Manchester, UK*

V. Blackmore, T. Carlisle, J.H. Cobb, W. Lau, M. Rayner [18], C.D. Tunnell, H. Witte [19], S. Yang

Department of Physics, University of Oxford, Denys Wilkinson Building, Oxford, UK
[18] *Now at DPNC, Université de Genève, Switzerland*
[19] *Now at Brookhaven National Laboratory, Upton, NY, USA*

C.N. Booth, P. Hodgson, L. Howlett, R. Nicholson, E. Overton, M. Robinson, P. Smith

Department of Physics and Astronomy, University of Sheffield, Sheffield, UK

D. Adey, J. Back, S. Boyd, P. Harrison

Department of Physics, University of Warwick, Coventry, UK

M. Ellis [20], P. Kyberd, M. Littlefield, J.J. Nebrensky

Brunel University, Uxbridge, UK
[20] *Now at Westpac Institutional Bank, Sydney, Australia*

A.D. Bross, S. Geer, D. Neuffer, A. Moretti, M. Popovic

Fermilab, Batavia, IL, USA

M.A.C. Cummings, T. J. Roberts

Muons, Inc., Batavia, IL, USA

A. DeMello, M.A. Green, D. Li, S. Virostek, M.S. Zisman

Lawrence Berkeley National Laboratory, Berkeley, CA, USA

B. Freemire, P. Hanlet, D. Huang[21], G. Kafka, D.M. Kaplan, P. Snopok, Y. Torun

Illinois Institute of Technology, Chicago, IL, USA
[21] *Now at Shangai Synchrotron Radiation Facility, Shangai, PR China*

S. Blot, Y.K. Kim

Enrico Fermi Institute, University of Chicago, Chicago, IL, USA

U. Bravar

University of New Hampshire, Durham, NH, USA

Y. Onel

Department of Physics and Astronomy, University of Iowa, Iowa City, IA, USA

D. Cline, Y. Fukui, K. Lee, X. Yang

Department of Physics and Astronomy, University of California, Los Angeles, CA, USA

R.A. Rimmer

Jefferson Lab, Newport News, VA, USA

L.M. Cremaldi, G. Gregoire [22],T.L. Hart, D.A. Sanders, D.J. Summers

University of Mississippi, Oxford, MS, USA
[22] *Permanent address Institute of Physics, Université Catholique de Louvain, Louvain-la-Neuve, Belgium*

L. Coney, R. Fletcher, G.G. Hanson, C. Heidt

University of California, Riverside, CA, USA

J.Gallardo, S. Kahn[23], H. Kirk, R.B. Palmer

Brookhaven National Laboratory, Upton, NY, USA
[23] *Now at Muons, Inc., IL, USA*

ABSTRACT: The international Muon Ionization Cooling Experiment (MICE), which is under construction at the Rutherford Appleton Laboratory (RAL), will demonstrate the principle of ionization cooling as a technique for the reduction of the phase-space volume occupied by a muon beam. Ionization cooling channels are required for the Neutrino Factory and the Muon Collider. MICE will evaluate in detail the performance of a single lattice cell of the Feasibility Study 2 cooling channel. The MICE Muon Beam has been constructed at the ISIS synchrotron at RAL, and in MICE Step I, it has been characterized using the MICE beam-instrumentation system. In this paper, the MICE Muon Beam and beam-line instrumentation are described. The muon rate is presented as a function of the beam loss generated by the MICE target dipping into the ISIS proton beam. For a 1 V signal from the ISIS beam-loss monitors downstream of our target we obtain a 30 KHz instantaneous muon rate, with a neglible pion contamination in the beam.

KEYWORDS: Muon Ionization Cooling; Neutrino Factory; Muon Collider; MICE; Muon Beam.

---

*Corresponding author. E-mail:Maurizio.Bonesini@mib.infn.it

Contents

1. Introduction **1**

2. The MICE concept **3**

3. MICE Muon Beam **7**
3.1 Overview 7
3.2 Beam-line elements and instrumentation 9
3.2.1 The MICE target 9
3.2.2 The MICE luminosity monitoring 9
3.2.3 The MICE Muon Beam magnets 11
3.2.4 The proton absorber 13
3.2.5 Diffuser 14
3.2.6 Beam-line diagnostics 15
3.3 Optimisation of the beam line 15
3.3.1 Downstream optimisation 16

4. The particle identification system in MICE Step I **17**
4.1 The Cherenkov counters 18
4.2 The TOF detectors 19
4.3 KL detector 23

5. The MICE Step I Trigger, Data Acquisition and Online/Offline Software **27**
5.1 Trigger and Data acquisition 27
5.2 The control system and online monitoring of MICE 29
5.3 The MICE Offline Software System 30

6. Characterisation of the MICE Muon Beam **30**
6.1 Particle rates and beam profiles in the MICE beam line 30

7. Conclusions **33**

---

1. Introduction

Muon storage rings have been proposed as sources of intense, high-energy neutrino beams [1, 2] and as high energy lepton-antilepton colliders [3, 4]. In each of these facilities, the volume of phase space occupied by the muon beam must be reduced (cooled) before the beam is accelerated and stored. The muon lifetime is so short that unacceptable decay losses will occur if conventional cooling techniques are employed [5]. Ionization cooling is fast, as the cooling is generated by ionization energy loss as the muon beam passes through an “absorber” material, the lost longitudinal momentum being restored in accelerating cavities. Ionization cooling has therefore been adopted in the proposed design for both the Neutrino Factory and the Muon Collider [6].

At the Neutrino Factory [2], intense beams of high energy neutrinos are produced from the decay of muons circulating in a storage ring. Long straight sections in the storage ring direct neutrino beams to one or more distant detectors. The energy spectrum and flavour composition of the beam are known precisely, as compared to those of conventional neutrino beams [7]. A number of conceptual designs for the Neutrino Factory have been proposed [8, 9, 10, 11, 12] each of which exploits an ionization-cooling channel to increase significantly the muon flux delivered to the storage ring. The baseline design for the facility being developed by the International Design Study for the Neutrino Factory (IDS-NF) collaboration delivers 10^{21} muon decays per year and has been shown to have a discovery reach that is significantly better than that of realistic alternatives. The cooling channel specified in the IDS-NF baseline delivers an increase of a factor 2.4 in the stored-muon flux and is essential for the design performance of the facility to be delivered.

The Muon Collider [13] offers an attractive route to multi-TeV lepton-antilepton collisions. Since the muon mass is 200 times that of the electron it is possible to deliver very high-energy beams using circular accelerators that can be designed to fit within the area of existing particle-physics laboratory sites. In addition, the large muon mass implies a reduction in the rate of beam-strahlung by a factor of $\sim 10^4$ over an e^+e^- collider of the same centre-of-mass energy. As a consequence, the annihilation-energy distribution is much narrower at a Muon Collider than at an e^+e^- collider of the same energy.

The $\mu^+\mu^-$ annihilation cross section falls rapidly as the centre-of-mass energy in the collision increases, therefore high luminosity ($\gtrsim 10^{34}\,\mathrm{cm}^{-2}\mathrm{s}^{-1}$) is critical to the success of the Muon Collider. To achieve the required luminosity, the muon-beam phase space must be cooled in all six phase-space dimensions: a reduction in the six-dimensional emittance by a factor $\sim 10^6$ being required. By contrast, the cooling requirements of the Neutrino Factory, which requires cooling of only the four-dimensional transverse phase space, are relatively modest.

Ionization cooling is accomplished by passing the muon beam through a low-Z material (the “absorber”) in which it loses energy through ionization. The energy loss results in a reduction in the longitudinal and the transverse components of momentum. The lost energy is restored by accelerating the beam such that the longitudinal component of momentum is increased while the transverse components remain unchanged. The net effect of these two operations is to reduce the divergence of the beam, thereby reducing the volume of transverse phase space it occupies. Beam transport through the absorber and the accelerating structures is achieved using a solenoid-focusing lattice.

The rate of change of normalised emittance due to ionization cooling in a medium of thickness X may be described as [6]:

$$\frac{d\varepsilon_N}{dX} \approx -\frac{\varepsilon_N}{\beta^2 E_\mu}\left\langle \frac{dE}{dX} \right\rangle + \frac{\beta_t (0.014\ \mathrm{GeV})^2}{2\beta^3 E_\mu m_\mu X_0}\,; \tag{1.1}$$

where ε_N is the normalised transverse (four-dimensional) emittance of the beam, X_0 is the radiation length of the medium, β_t is the betatron function, E_μ and m_μ the energy and mass of the muons and

$\beta = pc/E$ their velocity. The first (negative) term on the right hand side of equation 1.1 describes a reduction of emittance per unit length, i.e. cooling. The second (positive) term describes the heating effect of multiple scattering. The two effects reach an equilibrium when the emittance of the beam is:

$$\varepsilon_{eq} \approx \frac{\beta_t (0.014\ \mathrm{GeV})^2}{2\beta m_\mu X_0} \left\langle \frac{dE}{dX} \right\rangle^{-1} . \tag{1.2}$$

The ideal cooling channel will produce the lowest equilibrium emittance. This is obtained when β_t is minimised and $X_0 \cdot \left\langle \frac{dE}{dX} \right\rangle$ is maximised. To minimise β_t requires strong focusing at the absorber while hydrogen offers the largest value of $X_0 \cdot \left\langle \frac{dE}{dX} \right\rangle$.

While the principle of ionization cooling is readily described using equations 1.1 and 1.2, the construction of an ionization-cooling cell requires significant engineering. In a practical ionization-cooling cell, the energy loss in the absorber must be replaced by means of RF cavities: momentum must be restored so that beam transport through subsequent cells is unaffected.

The international Muon Ionization Cooling Experiment (MICE) [14, 15] is being constructed at the Rutherford Appleton Laboratory (RAL). The experiment will consist of the full cell of an ionization-cooling lattice and the instrumentation necessary to measure the emittance of a muon beam before it enters and after it leaves the cell. In this way, the MICE collaboration will measure the cooling performance of the lattice cell in a variety of modes of operation and over a range of momentum and emittance. The results of the experiment will allow the cooling channels of the Neutrino Factory and Muon Collider to be optimised.

2. The MICE concept

A schematic diagram of the MICE experiment is shown in figure 1. The MICE cooling channel, which is based on a single lattice cell of the cooling channel described in [8], comprises three volumes of ~ 20 litre of liquid hydrogen and two linac modules each consisting of four 201 MHz cavities, with gradients of ~ 10 MV/m. Beam transport is achieved by means of a series of superconducting solenoids: the "focus coils" focus the beam into the liquid-hydrogen absorbers, while a "coupling coil" surrounds each of the linac modules.

Detailed Monte Carlo simulations of the passage of muons through the cooling cell have been carried out to estimate its performance. The results indicate that a reduction in the normalised emittance of 10% is expected for a muon beam entering the cell with a momentum of 200 MeV/c and an emittance $\varepsilon_N = 6.2\pi$ mm·rad. The instrumentation upstream and downstream of the cooling cell is required to measure this change in emittance, $\Delta\varepsilon_N$, with a relative precision $\Delta\varepsilon_N/\varepsilon_N = 1\%$; i.e., measurements of ε_N upstream and downstream of the cooling cell with an absolute precision of 0.1% are required, to allow the extrapolation to a full cooling channel. Conventional emittance measurement techniques based on beam-profile monitors do not have the required precision.

While the muon-beam intensity in the ionization-cooling channel at the Neutrino Factory and the Muon Collider is in excess of $10^{14}\,\mu^{\pm}$/s, the phase-space density is always low enough for space-charge forces to be neglected. This fact has been exploited to devise a single-particle experiment in which each muon is measured using state-of-the-art particle detectors and the bunched muon-beam is reconstructed offline. The instrumentation upstream of the MICE cooling cell

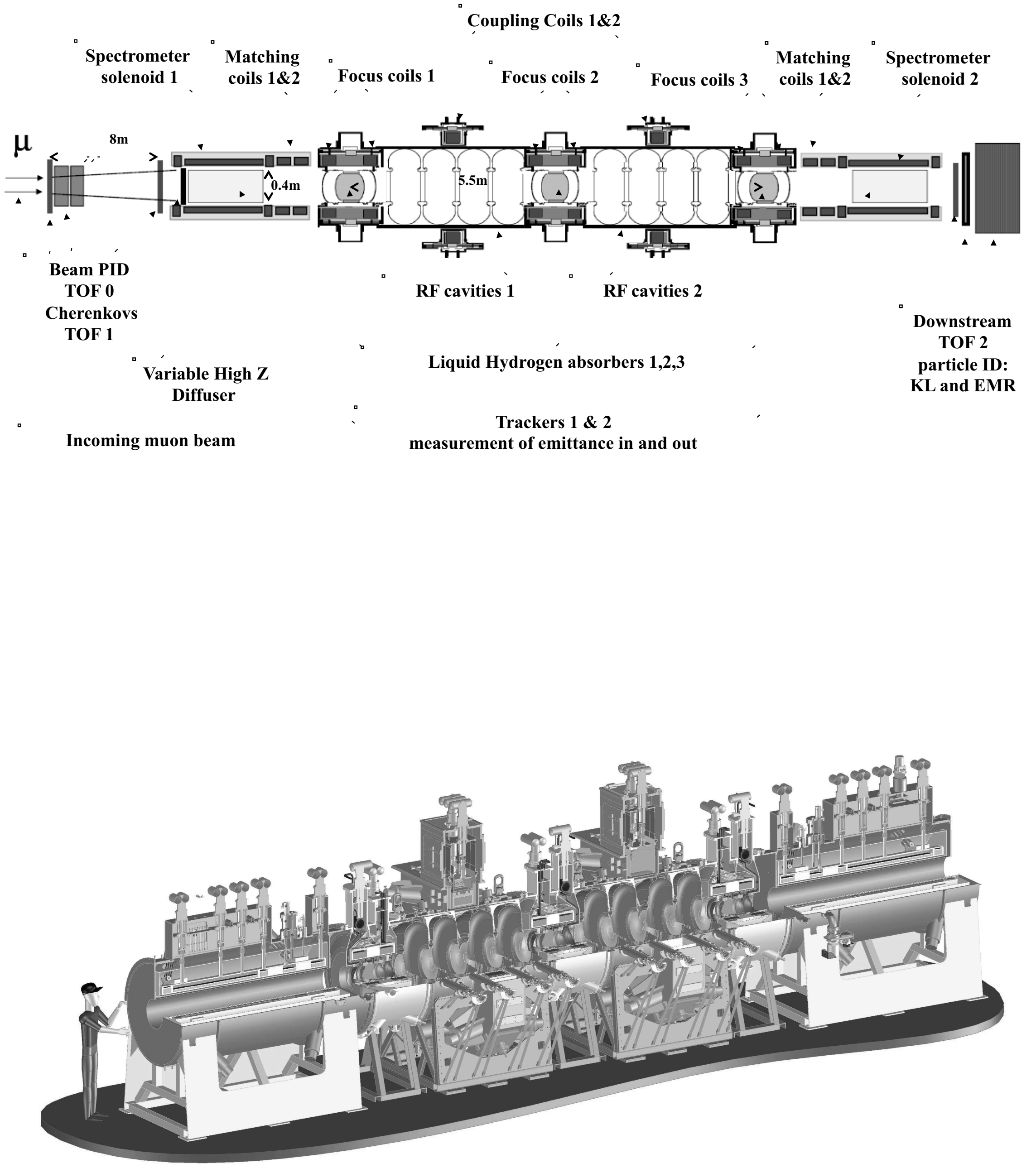
Coupling Coils 1&2
Spectrometer solenoid 1
Matching coils 1&2
Focus coils 1
Focus coils 2
Focus coils 3
Matching coils 1&2
Spectrometer solenoid 2
μ
8m
0.4m
5.5m
Beam PID
TOF 0
Cherenkovs
TOF 1
RF cavities 1
RF cavities 2
Downstream
TOF 2
particle ID:
KL and EMR
Variable High Z Diffuser
Liquid Hydrogen absorbers 1,2,3
Incoming muon beam
Trackers 1 & 2
measurement of emittance in and out

Figure 1. Top panel: view of the MICE experimental set-up; the cooling channel, with its three liquid hydrogen absorbers and two RF cavity modules, is sandwiched between two identical trackers. The sequence of solenoids defining the MICE optics is also visible. The muon beam is coming from the left. Bottom panel: 3D cut-away engineering drawing of MICE, starting at first Spectrometer Solenoid. Beam instrumentation is not shown.

includes a particle-identification (PID) system (scintillator time-of-flight hodoscopes TOF0 and TOF1 and threshold Cherenkov counters Ckova and Ckovb) that allows a pure muon beam to be selected. Downstream of the cooling channel, a final hodoscope (TOF2) and a calorimeter system allow muon decays to be identified and rejected. The calorimeter system is composed of a lead-scintillator section (KL), similar to the KLOE [16] design but with thinner lead foils, followed by a fully active scintillator detector (the electron-muon ranger, EMR) in which the muons are brought to rest. Charged-particle tracking in MICE is provided by two solenoidal spectrometers. The MICE instrumentation must be sufficiently robust to perform efficiently in the presence of background induced by X-rays produced in the RF cavities. For a full description of the experiment see [15].

The position, momentum and energy of each muon is measured before and after the cooling cell. For each particle x, y, t, $x' = dx/dz = p_x/p_z$, $y' = dy/dz = p_y/p_z$ and $t' = dt/dz = E/p_z$ are measured; p_i is the i^{th} component of momentum, E is the energy and the MICE coordinate system is defined such that the z axis is parallel to the nominal beam axis, the y axis points vertically upward and the x axis completes a right-handed coordinate system. The time, t, corresponds to the moment the particle crosses a reference surface within the tracking volume. The input and output normalised emittances, ε_{N_i} and ε_{N_o}, of a beam of N muons can be determined from the measurements of the phase-space coordinates of single muons in the up- and down-stream trackers. Because they are measured for the same ensemble of muons, ε_{N_i} and ε_{N_o} will be correlated with the effect of reducing the statistical error on the fractional change in emittance, $f = (\varepsilon_{N_i} - \varepsilon_{N_o})/\varepsilon_N$, below $1/\sqrt{N}$. The only stochastic process is multiple scattering in the absorbers and it can be shown that [17]

$$\sigma_f^2 = \frac{1}{2N}\frac{\bar{p}_s^2}{\bar{p}_t^2} \tag{2.1}$$

where $\bar{p}_t^2$ is the mean square transverse momentum of the beam at the absorbers and $\bar{p}_s^2$ is the mean square transverse momentum kick due to multiple scattering. It has been demonstrated with Monte Carlo studies [18] that for beams with $\varepsilon_N > 3\pi\,\text{mm}\cdot\text{rad}$ a sample of 3×10^5 muons is sufficient to reduce the statistical error on f to less than one percent.

The MICE Muon Beam is required to deliver beams with a pion contamination below 10% and a central momentum (p_μ) in the range $140 \le p_\mu \le 240\,\text{MeV/c}$. The beam line must also deliver a transverse emittance in the range $3 \le \varepsilon_N \le 10\ \pi\,\text{mm}\cdot\text{rad}$. The full range of emittance is required over the full range of momentum. A tungsten or brass "diffuser" of variable thickness is placed at the entrance to the upstream spectrometer solenoid to generate the divergence necessary for the required range of emittance.

At a rate of $\sim 30\,\mu/\text{s}$ a sample of 10^5 muons may be accumulated in one hour, giving the possibility to record all the needed momentum/emittance beam settings in the available running time.

The MICE program was conceived to be carried out in six "Steps", summarised in table 1 and figure 2. A thorough description of all MICE Steps is beyond the scope of this paper. However, each Step requires that the MICE Muon Beam meets the specifications outlined above. Step I, in which the muon beam was characterized using the time-of-flight (TOF), Cherenkov and KL detectors, was completed in August 2010. The EMR calorimeter [19], that will complete the downstream calorimetry, will follow soon.

Table 1. The six "Steps" in which it was conceived to carry out the MICE programme. The physics programme of steps II to III will be carried out within the STEP IV configuration.

Step	Description
I	Beam characterisation and detector calibration.
II	Upstream spectrometer and diffuser. Incoming beam emittance can be changed and measured precisely.
III	Downstream spectrometer: study of systematics in emittance measurement in the two spectrometers. Solid absorber with measurement of energy loss and multiple scattering correlations.
IV	Introduction of the first liquid hydrogen absorber and focus-coil module.
V	First linac section and second hydrogen absorber/focus-coil module. First measurement of cooling with momentum recovery.
VI	Second linac module and third liquid hydrogen absorber/focus-coil module. Measurement of emittance before and after the cooling cell, in various optics configurations, with momentum recovery.

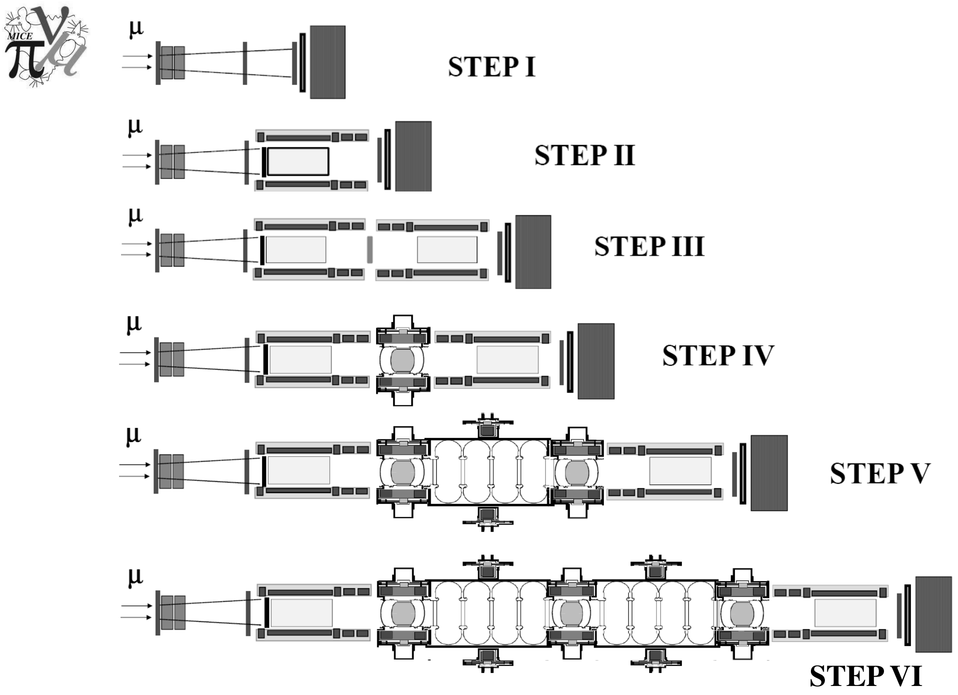

Figure 2. Schematic diagrams of the six "Steps" in which the MICE programme was conceived.

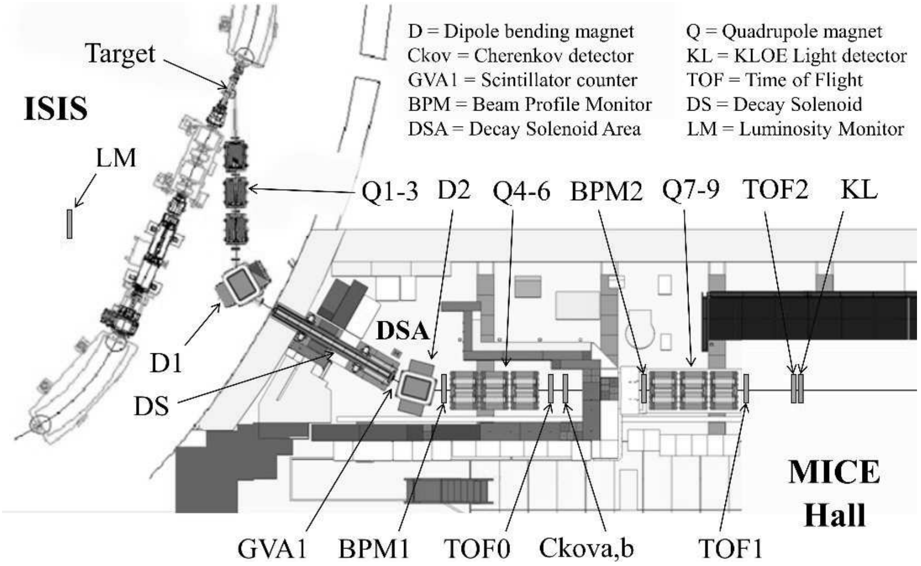
D = Dipole bending magnet
Ckov = Cherenkov detector
GVA1 = Scintillator counter
BPM = Beam Profile Monitor
DSA = Decay Solenoid Area
Q = Quadrupole magnet
KL = KLOE Light detector
TOF = Time of Flight
DS = Decay Solenoid
LM = Luminosity Monitor
Target
ISIS
LM
Q1-3
D2
Q4-6
BPM2
Q7-9
TOF2
KL
DSA
D1
DS
MICE
Hall
GVA1
BPM1
TOF0
Ckova,b
TOF1

Figure 3. Top view of the MICE beam line with its instrumentation, as used in Step I.

3. MICE Muon Beam

3.1 Overview

The design of the MICE Muon Beam is similar to that of the μE4 beam line at the Paul Scherrer Institute (PSI) in Switzerland. The MICE Muon Beam may be divided, conceptually, into three sections (see figure 3). In the upstream section, pions produced by the ISIS proton beam striking a titanium target are captured using a quadrupole triplet (Q1–3). The pions are transported to a bending magnet (D1) which directs pions of particular momentum into the decay solenoid (DS). The decay solenoid, the second section of the beam line, causes the pions to spiral around the nominal beam axis, increasing the path length. This effect together with the solenoid focusing increases the number of muons captured between D1 and the second dipole magnet (D2). D2, the first element of the downstream section, directs muons of a particular momentum into a quadrupole channel (Q4–6 and Q7–9) that transports the muon beam to the MICE experiment.

The composition and momentum spectrum of the beam delivered to MICE is determined by the interplay between the two bending magnets D1 and D2. This is illustrated in figure 4. With D1 set to select a particular pion momentum, p_{D1} (horizontal axis), the kinematics of pion decay result in muons with momentum in the range $p_{\mu\,\mathrm{min}} \leq p_\mu \leq p_{\mu\,\mathrm{max}}$. The kinematic limits are indicated in figure 4. For $p_{D1} \gtrsim 200\,\mathrm{MeV/c}$, $p_{\mu\,\mathrm{max}} \sim p_{D1}$. When D2 is set to select particles with momentum $p_{D2} \sim p_{\mu\,\mathrm{min}}$, backward-going muons in the pion rest frame are selected. The muon-beam purity, P_μ, is defined as $P_\mu = N_\mu / N_T$, where N_μ is the number of muons in the beam and N_T is the total number of particles. A muon beam of sufficient purity can be selected by setting $p_{D2} = p_{\mu\,\mathrm{min}} \sim p_{D1}/2$. This can be seen in the right-hand panel of figure 4 where the momentum spectra of particles emerging from the decay solenoid are plotted in a simulation in which D1 was set to select a central momentum of 400 MeV/c. The figure shows that setting D2 to select a momentum bite of 10% around $p_{D2} = 236\,\mathrm{MeV/c}$ delivers a muon beam with a pion contamination (defined as N_π / N_T, where N_π is the number of pions in the beam) less than 2%. In practice, a muon

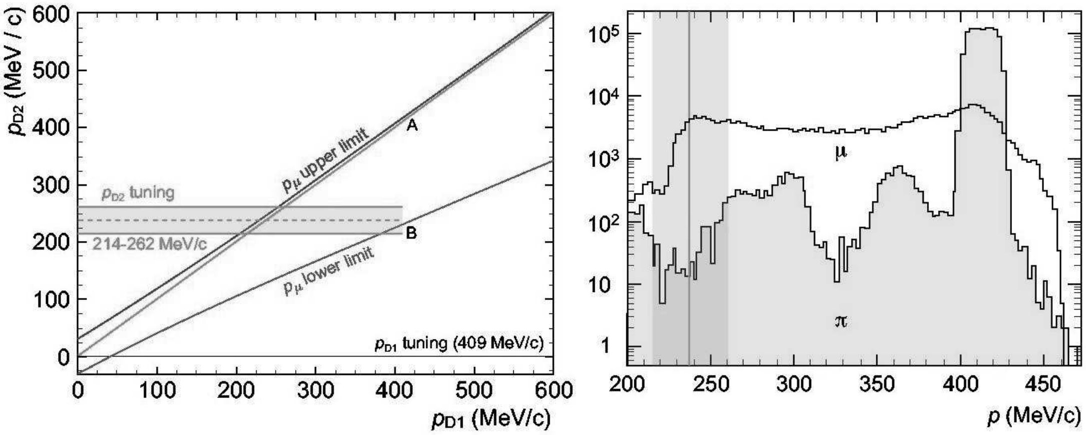

Figure 4. Working principle of the MICE beam line. Left-hand panel: the red and blue lines are the kinematic limits of the spectrum for muons produced in pion decays. By tuning D2 to the backward going muon peak an almost pion-free sample is produced. Right-hand panel: simulation showing pion and muon spectra at the end of the decay solenoid. Only high momentum pions survive. The green band shows the acceptance of D2, when tuned to the backward-going muon peak.

beam with a purity in excess of 95% is obtained by setting $p_{D1} \simeq 2p_{D2}$. This case is referred to as "$\pi \to \mu$ mode". A momentum-selected beam containing pions, muons, protons and electrons (or positrons) can be obtained by setting $p_{D1} \simeq p_{D2}$. Such a setting is referred to as "calibration mode" and is used for the calibration of detectors.

The muon beams delivered to MICE are characterized by their normalised emittance, ε_N, and momentum, p_z. Different beam settings are identified using the notation (ε_N, p_z), where ε_N is measured in π mm · rad and p_z in MeV/c. The "nominal" values of ε_N and p_z are defined such that the nominal value of ε_N is evaluated in the upstream spectrometer solenoid and the nominal value of p_z is evaluated at the centre of the central liquid-hydrogen absorber in the Step VI configuration. The baseline optics deliver a beam characterized by $(\varepsilon_N, p_z) = (6, 200)$. The (ε_N, p_z) space is discretised into a matrix of nine elements (see table 4). Each cell of this emittance-momentum matrix is associated with a specific downstream beam-line optics. Together the cells span the (ε_N, p_z) space required to serve the entire MICE programme.

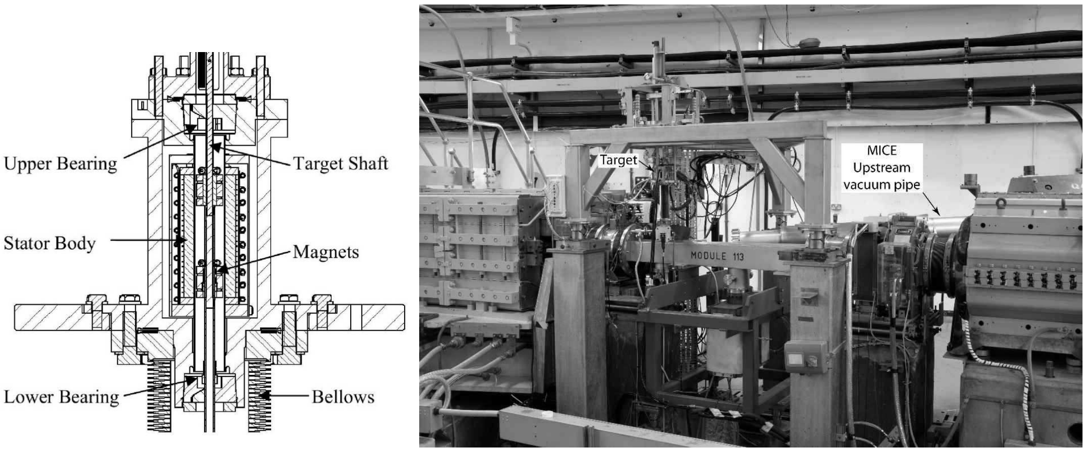

Figure 5. Left panel: MICE target drive schematics. Right panel: The MICE target installed in ISIS.

3.2 Beam-line elements and instrumentation

3.2.1 The MICE target

Protons are injected into ISIS with a kinetic energy of 70 MeV and are accelerated over a period of 10 ms up to 800 MeV at a repetition rate of 50 Hz [1]. The MICE target has been designed to dip into the beam shortly before extraction at a rate of $\sim$ 1 Hz, i.e. sampling one in 50 of the ISIS beam pulses.

The MICE target is a hollow titanium cylinder with an outer diameter of 6 mm and an inner bore of 4.6 mm. The target dips vertically into the beam, intercepting it over the last 3 ms of the acceleration cycle ($\sim$ 4 000 turns). Over this period, the target samples proton-beam energies in the range 617–800 MeV. The beam envelope shrinks as the beam is accelerated.

To insert the target into the shrinking beam envelope requires an acceleration of $\sim 80\ g$. The target-insertion mechanism consists of a linear electromagnetic motor in which permanent magnets mounted on the target shaft are accelerated by a series of 24 coils contained within the stator. An optical position-sensing system with laser quadrature readout is used to monitor the position of the shaft and to control the drive current to the 24 coils (see left-hand panel of figure 5). A paper describing the design and operation of the MICE target is in preparation [20].

3.2.2 The MICE luminosity monitoring

There are 39 beam loss monitors (BLM) [21] placed around the inner radius of ISIS. These are argon-filled cylindrical ionization chambers, 3 m long, 16 mm in diameter and situated 2–3 m from the beam axis parallel to the beam. The BLMs detect particles produced by protons that are lost from the beam envelope and interact with accelerator components. The ionization chambers that form the BLMs produce a voltage signal proportional to the particle rate. This signal is integrated over some time interval (typically between 1 and 3 ms) to give an overall measure of beam loss (in units of V$\cdot$ ms). The ISIS synchrotron lattice has 10 "super periods", numbered from 0 to 9,

---

[1] Upon reaching 800 Mev energy the protons are extracted to the ISIS neutron-production targets.

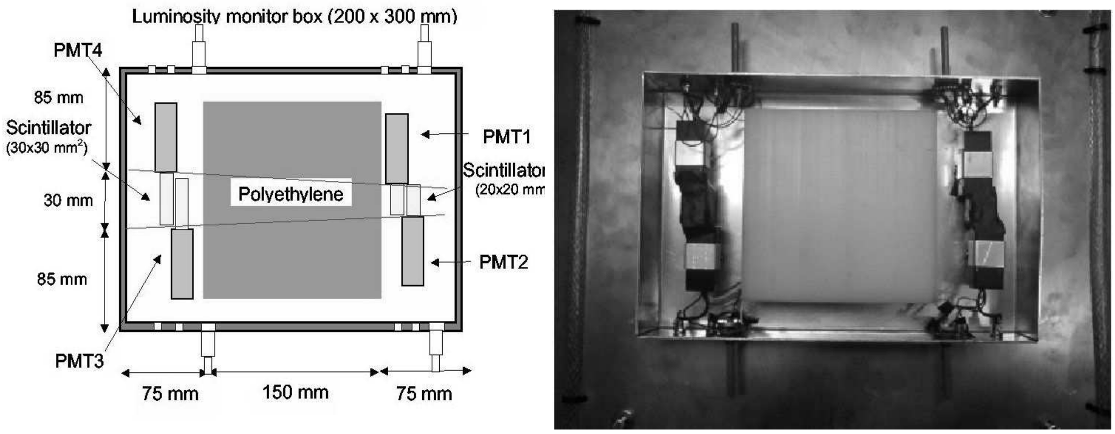

Figure 6. Left panel: Luminosity Monitor design schematic (particles from the beam travel from right to left). Right panel: photograph of the detector.

with the MICE target situated in super period 7 (SP7). The signal from the four BLMs in SP7 is a measure of beam loss produced by the MICE target.

The MICE Luminosity Monitor (LM) provides a measurement of the particle rate close to the MICE target independent of the ISIS Beam Loss Monitors. The LM is located inside the ISIS synchrotron ring, 10 m from the target (see figures 3 and 8). A line drawn from the target to the LM makes an angle of 25° with respect to the direction of the proton beam at the target. The LM therefore samples particles at an angle similar to that at which particles are captured by Q1–3. The rate recorded by LM may therefore be used to validate the simulation of the upstream beam line and to normalise the rates measured in the beam line instrumentation to the number of protons on target (POT).

The LM consists of two pairs of small scintillators placed either side of a polyethylene block that absorbs protons with momentum below ~ 500 MeV/c and pions with momentum below ~ 150 MeV/c (see figure 6). The scintillators are read out by Hamamatsu H5783P low noise PMTs which have a rise time of 0.8 ns and a gain of 10^5 [22]. Upstream of the polyethylene block, PMTs 1 and 2 are bonded to scintillator blocks of dimension $20 \times 20 \times 5\,\mathrm{mm}^3$; downstream, PMTs 3 and 4 are attached to $30 \times 30 \times 5\,\mathrm{mm}^3$ scintillator blocks. Neutrons may be detected if scattering inside the polyethylene block releases a proton. The PMT signals are fed to LeCroy 623B NIM octal discriminators, the three outputs of which are used to form three coincidence signals using a LeCroy 622 NIM quad coincidence unit [23]. Coincidences are recorded within the experimental trigger gate during each spill: PMTs 1 and 2 (LM12), 3 and 4 (LM34) and all four PMTs (LM1234) [2].

The quad LM1234 coincidence rate is plotted as a function of beam loss in figure 7. The data show an approximately linear relation between LM counts and beam loss in SP7 between 0.5 V·ms and 3 V·ms. Due to beam losses not caused by the MICE target, the relation below 0.5 V·ms becomes not linear. Above 3 V·ms saturation effects become significant. The rate recorded by

---

[2] In the following, we use the term "spill" for the burst of particles resulting from one target dip, even though the primary ISIS proton beam is not extracted in producing the MICE beam.

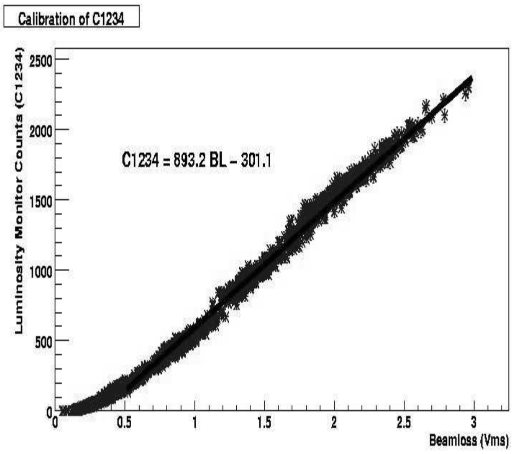

Figure 7. Luminosity monitor data showing a direct relationship between luminosity and beam loss on all three scalar output channels. Graphs show counts for coincidences of signals for PMTs 1,2,3 and 4. The straight lines are a linear fit to the data between 0.5 V· ms and 3 V· ms.

the Luminosity Monitor has been used to convert integrated beam loss to protons on target (POT) [24, 25].

3.2.3 The MICE Muon Beam magnets

The quadrupole magnets that form the upstream pion-capture section of the upstream beam line are Type-IV quadrupoles recovered from the NIMROD accelerator which operated at RAL during the 1960s and 1970s [26]. Q1–3 have a circular aperture at the pole tips of 203 mm. The operating field gradients, shown in table 2, are always significantly smaller than the maximum gradient of 10 T/m. The power to each quadrupole is provided by a 200 A, 30 V power supply. An aluminium vacuum pipe passes through Q1–3 and extends into a vacuum box inside D1.

The quadrupoles that form the two downstream triplets (Q4–6 and Q7–9) are each Type QC quadrupoles from DESY [26]. The downstream quadrupoles have cross-shaped apertures, with a circular aperture of 352 mm diameter at the pole tips and a maximum gradient of 8 T/m. They are each excited by a 400 A, 70 V power supply.

The two dipoles (D1, D2) are large, 17 t, rectangular NIMROD Type-1 dipoles [26]. The nominal apertures for these magnets are rectangular with tapered pole pieces that provide a 6 inch vertical aperture and a 20 inch horizontal aperture. D1 is operated at a field close to saturation of the iron yoke. The power supply for this magnet is limited for operation at a maximum current of 440 A at 240 V. D2 is operated at a more modest field and is excited with a power supply delivering 200 A at 100 V.

The large superconducting decay solenoid (DS) was supplied by the Paul Scherrer Institute (PSI) in Switzerland, where it had been in use at the μE4 beam line from 1974 to 2004 [27]. The coils which make up the DS have an open inner radius of 57.5 mm (outer radius 65 mm) and a length of 5 m. The conductor is a Cu/NbTi mixture with proportions Cu:NbTi of 3.5:1. The magnet has a stored energy of 1.5 MJ. The DS can operate at a maximum current of 1000 A, with a current

Table 2. Beam-line magnet physical properties.

Beam line Magnet	Physical length (mm)	Aperture (mm)	Typical field (limit)
Quad Type-IV	1143	203 ϕ	1.6 (10) T/m
Quad Type QC	1170	352 ϕ	2 (8) T/m
Dipole Type-1 $6''$	1400	508 (H)$\times$ 152 (V)	1.47 (1.5) T
PSI Decay Solenoid	5000	115 ϕ	5 (5.7) T

density of 220 A mm^{-2}. The nominal operating field in MICE is 5 T, corresponding to a current of 870 A.

A summary of the position and dimensions of all the components along the MICE beam line is presented in table 3. A photograph of the upstream section of the beam-line is shown in figure 8 and of the downstream beam line in figure 9.

Table 3. The MICE beam-line elements and detectors for Step I.

Element	Distance from target [along nominal beam axis]	L_{eff}	Max field/gradient		Aperture Radius (Pole tip)	1/2-aperture [H/V]	
	(mm)	(mm)	(T)	(T/m)	(mm)	mm	mm
Q1	3000.0	888	-	1.6	101.5		
Q2	4400.0	888	-	1.6	101.5		
Q3	5800.0	888	-	1.6	101.5		
D1	7979.1	1038	1.6	-		254.0	76.0
Decay Solenoid	12210.7	5000	5.7	-	57.5		
Proton absorber	14880	Plastic sheets 15, 29, 49, 54 mm					
GVA1	15050.0	Scintillation counter (0.02 X_0)					
D2	15808.1	1038	0.85	-		254.0	76.0
BPM1	16992.0	Scintillating fibres (0.005 X_0)					
Q4	17661.6	660	-	2.3	176.0		
Q5	18821.6	660	-	2.3	176.0		
Q6	19981.6	660	-	2.3	176.0		
TOF0	21088.0	Segmented scintillator (0.12 X_0)					
Ckova	21251.5	Aerogel threshold Cherenkov (0.019 X_0)					
Ckovb	21910.9	Aerogel threshold Cherenkov (0.031 X_0)					
BPM2	24293.7	Scintillating fibres (0.005 X_0)					
Q7	25293.7	660	-	2.3	176.0		
Q8	26453.7	660	-	2.3	176.0		
Q9	27613.7	660	-	2.3	176.0		
TOF1	28793.1	Segmented scintillator (0.12 X_0)					
TOF2	31198.1	Segmented scintillator (0.12 X_0)					
KL	31323.1	Lead + scintillator (2.5 X_0)					
Tag counters	31423.1	Scintillation bars (0.06 X_0)					

The MICE beam line works with both positively and negatively charged muons. The change-over is achieved by physically disconnecting and swapping over the magnet power-supply cables.

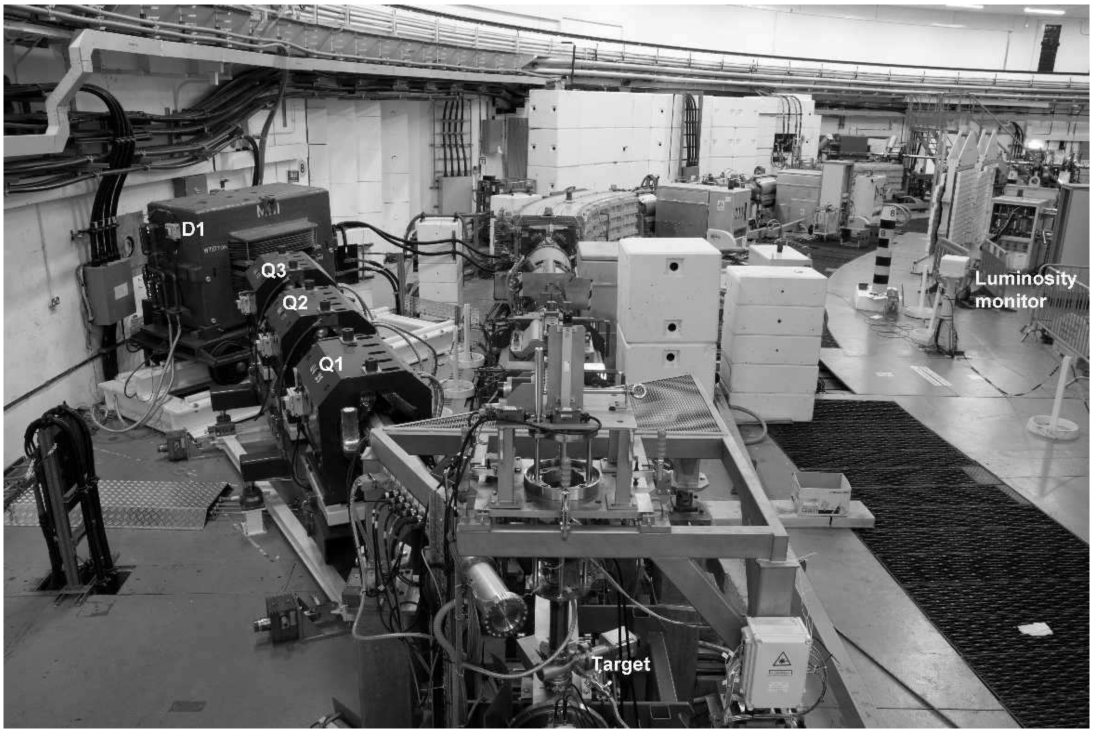

Figure 8. Upstream beam line. The target may be seen in the foreground of the photograph. The magnets that make up the upstream beam line (Q1–3 and D1) lie to the left of straight 7 of the ISIS proton synchrotron which can be seen in the centre of the figure. The luminosity monitor, surrounded by its white, borated-polythene shielding may be seen close to the right-hand edge of the photograph.

A simple system for monitoring and recording the operating polarity of the two bending magnets (and by inference the other beam-line elements) has been deployed [28] consisting of a pair of Honeywell LOHET-II Hall-effect sensors that are operating past saturation when placed in the dipole bores, even at minimal field strengths, and thus return one of the two well-defined voltages corresponding to the two possible polarities of each magnet.

3.2.4 The proton absorber

With the beam line set to transport positive particles, a large flux of protons is observed to exit the decay solenoid. The range of proton momenta selected by D1 is such that a large fraction of the protons reaching D2 will be accepted by Q4–6. As a result, unless action is taken to remove protons from the beam as it enters D2, an unacceptably large flux of protons would be transported to TOF0. In the momentum range of interest, the energy loss per unit length of material traversed is larger for protons than for pions. Borated-polyethylene sheets placed in the beam as it emerges from the decay solenoid are used to remove the protons. The boron loading of the polyethylene serves to increase the absorption rate of neutrons. The sheets have thicknesses of 15 mm, 29 mm, 49 mm and 54 mm and are raised and lowered into the beam using a cable-pull mechanism. The absorbers can be operated together or independently. When all four absorbers are placed in the beam, the 147 mm of material is enough to stop protons with momentum up to $\sim 500\,\text{MeV/c}$.

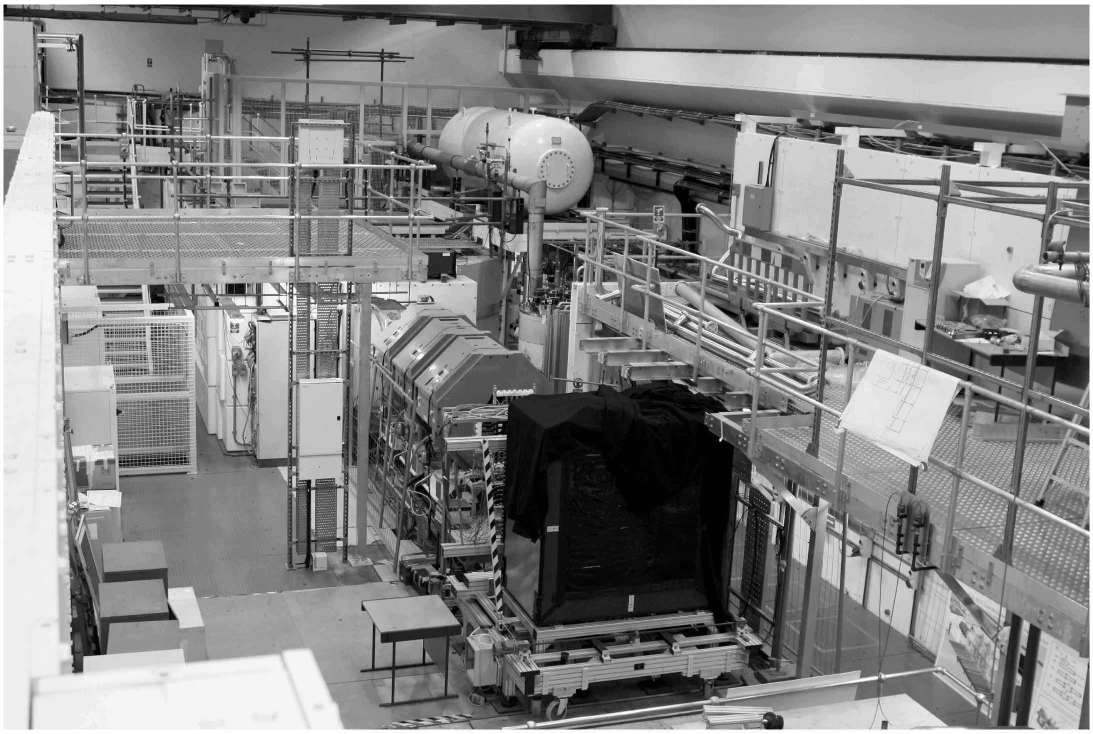

Figure 9. Downstream beam line. The ISIS synchrotron lies behind the curved wall in the background. The downstream quadrupoles (blue, hexagonal magnets) may be seen just downstream of the white concrete shielding. The time-of-flight counter TOF1 is seen immediately downstream of the final quadrupole. TOF1 is followed by the KL and the prototype EMR.

The choice of absorber thickness depends on the required muon-beam momentum. In a beam line set to deliver a nominal muon momentum of 140 MeV/c, D1 is set to select 360 MeV/c particles. In this case, a proton-absorber thickness of 44 mm is required to reduce the proton contamination in the muon beam delivered to MICE to less than 1%. The beam-line tune that delivers the nominal muon momentum of 240 MeV/c requires that D1 be set to select particles with a momentum of 507 MeV/c, and the full 147 mm proton-absorber thickness is then required to reduce the proton contamination to the few-% level. Pure positive muon beams of intermediate momentum are delivered using appropriate combinations of the four sheets.

3.2.5 Diffuser

The final element of the downstream section of the beam line is the diffuser. By introduction of material with a large radiation length into the beam, multiple Coulomb scattering increases the divergence of the beam, enlarging the emittance and providing an approximately matched beam in the upstream spectrometer solenoid. Since the diffuser must operate in the field of the 4 T spectrometer, electric motors and other magnetic components cannot be used. The diffuser design consists of a stainless steel drum, which is inserted into the upstream section of the first spectrometer solenoid [29]. The drum contains four irises, two of brass (2.97 mm, $0.2\,X_0$, and 5.94 mm, $0.4\,X_0$ thick) and two of tungsten (2.80 mm, $0.8\,X_0$, and 5.60 mm, $1.6\,X_0$). By selecting different combinations of irises, one can achieve a total of $3\,X_0$ in steps of $0.2\,X_0$. Each iris consists of two planes of four segments of material, supported by a Tufnol [30] ring of radius 100 mm (see figure 10) and is operated by a non-magnetic, air-driven actuator. The position of each iris is monitored by a set of optical sensors. When closed, the iris inserts solid petals into the beam; when it is open, the petals are stowed away within the Tufnol ring.

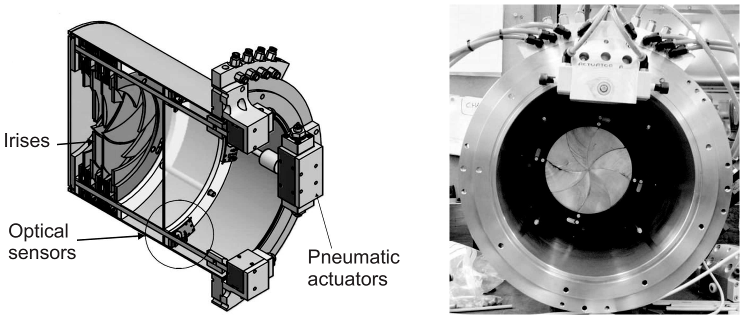

Figure 10. Left panel: schematic of the MICE diffuser showing the irises. Right panel: one of the brass irises being tested.

3.2.6 Beam-line diagnostics

The downstream beam line is instrumented with a scintillation counter (GVA1), placed just after the proton absorber, upstream of D2. GVA1 consists of a single slab of scintillator with $18 \times 18\,\text{cm}^2$ active area and 1 cm thickness, read out by a 2 inch EMI photomultiplier. Two Beam Profile Monitors mounted on the upstream faces of Q4 (BPM1) and Q7 (BPM2) were used to measure particle rate and beam position. The BPMs each comprise two planes of Kuraray 1 mm scintillating fibres. BPM1 has an area of $20 \times 20\,\text{cm}^2$, while BPM2 has an area of $45 \times 45\,\text{cm}^2$. The layers of optical fibres are supported by a sheet of Rohacell [31] foam 2.55 mm thick. An aluminium box encases the BPMs, except in the acceptance region of the fibres where four layers of Tedlar [32] keep the BPM light-tight. The light from the fibres is read out by two 64-channel multi-anode Burle [33] 85011-501 photomultiplier tubes (one per plane). Further details on both GVA1 and the BPMs are found in table 3.

3.3 Optimisation of the beam line

The upstream and downstream sections of the beam line are loosely coupled, allowing each section to be optimised independently. In the upstream section, where pions travel through an evacuated beam pipe, the matrix-evolution code TRANSPORT [34, 35] was therefore used to perform the optical design. In the decay solenoid, pion decay must be simulated and in the downstream beam